

Incident-energy dependence of the fragmentation mechanism reflecting the cluster structure of the ^{19}B nucleus

Hiroki Takemoto

Advanced Science Research Center, Japan Atomic Energy Research Institute, Tokai, Ibaraki 319-1195, Japan

Hisashi Horiuchi

Department of Physics, Kyoto University, Kyoto 606-8502, Japan

Akira Ono

Department of Physics, Tohoku University, Sendai 980-8578, Japan

(Received 7 September 2000; published 21 February 2001)

We investigate the fragmentation mechanism reflecting the cluster structure of the ^{19}B nucleus. We perform antisymmetrized molecular dynamics (AMD) calculations of $^{19}\text{B} + ^{14}\text{N}$ and $^{13}\text{B} + ^{14}\text{N}$ reactions, and compare ^{19}B fragmentation with ^{13}B fragmentation. The neutron drip-line nucleus ^{19}B has been predicted to have a well-developed cluster structure in its ground state while the neutron closed-shell nucleus ^{13}B has no clustering features in its structure. The clustering structure of ^{19}B is reflected in its fragmentation as the dynamical cluster breakup into He and Li isotopes, depending on the incident energy. In the low-incident-energy region around 30 MeV/nucleon, dynamical cluster breakup of ^{19}B occurs and brings about an abundance of He and Li isotopes in ^{19}B fragmentation compared with those in ^{13}B fragmentation. In the high-incident-energy region above 50 MeV/nucleon, dynamical cluster breakup of ^{19}B hardly occurs and the cluster structure of the ^{19}B nucleus is not reflected in its fragmentation. We suggest here the coincident experiment between He and Li isotopes as an experimental way to confirm whether the ^{19}B nucleus has a cluster structure in its ground state or not.

DOI: 10.1103/PhysRevC.63.034615

PACS number(s): 25.60.-t, 25.70.Mn, 21.60.Gx, 24.10.Cn

I. INTRODUCTION

The amount of experimental information regarding nuclei far from the stability line has been increased greatly by means of unstable nuclear beams [1–3]. Recently obtained data of neutron-rich B isotopes display an interesting dependence of electric and magnetic moments on the neutron number N [4,5]. It is expected that the N dependence of the electromagnetic properties is caused by some structure change, such as the development of cluster structure. The possibility of clustering structure in neutron-rich B isotopes has been theoretically suggested in a pioneering work with the molecular-orbital model [6,7]. In this model, B-isotope systems are described as being composed of an α - α core surrounded by neutrons and a proton. It was found that the optimum distance of the α - α core of the B isotope became larger with an increase of neutron number N in the $N > 8$ region.

Recently, the structure of odd-even B isotopes up to the neutron drip line was studied systematically with antisymmetrized molecular dynamics (AMD) [8]. Binding energies and other observed data of B isotopes are reproduced by the AMD method quite well, and, in particular, a very good reproduction of electromagnetic properties is obtained. The behavior of electromagnetic properties has been explained in terms of the drastic structure change from shell-model-like structure to clustering structure; namely, the neutron closed-shell nucleus ^{13}B possesses shell-model-like structure and cluster structure develops with an increase of N beyond $N = 8$. This explanation gives us an important indication that

the clustering structure in neutron-rich B nuclei is strongly suggested by the experimental data.

As far as experimental investigation of clustering structure in neutron-rich nuclei is concerned, an exotic molecular structure of excited states in the ^{12}Be nucleus has been reported by Freer *et al.* [9]. They have studied the breakup of ^{12}Be into $^6\text{He} + ^6\text{He}$ and $^4\text{He} + ^8\text{He}$, and the measurements indicate that breakup occurs from rotational states in the 10–25 MeV excitation energy with spins in the range of $4\hbar$ – $8\hbar$. The inferred moment of inertia is consistent with the cluster decay of an exotic molecular structure of the ^{12}Be nucleus with an α - $4n$ - α cluster configuration. But it has not been yet confirmed experimentally whether or not the ^{19}B nucleus has a clustering structure in its ground state.

In this paper we investigate the fragmentation mechanism reflecting the cluster structure of the ^{19}B nucleus in its ground state with the AMD method, and suggest an experimental way to verify the cluster structure of ^{19}B by the use of the fragmentation reaction. In order to study this kind of subject, the model should be able to describe both nuclear reactions and nuclear structure. For investigating various kinds of reaction mechanism and also an unknown reaction mechanism in heavy-ion reactions systematically, microscopic simulation studies, such as the Boltzmann-Uehling-Uhlenbeck (BUU) and Vlasov-Uehling-Uhlenbeck (VUU) methods [10] and quantum molecular dynamics (QMD) [11], are very useful since they do not assume any reaction mechanisms. However, most of them are not suitable for the study of the fragmentation mechanism reflecting the nuclear structure, because these models are of a semiclassical character

and cannot describe quantum mechanical features such as the shell effect in heavy-ion reactions. On the other hand, in AMD [12], the system is described with a fully antisymmetrized wave function (a Slater determinant of Gaussian wave packets), and therefore the ground states of initial nuclei are most precisely described among many simulation methods. In fact, as mentioned above, AMD has been successfully applied to nuclear structure problems [8,13,14] such as the structure change from shell-model-like structure to clustering structure. Furthermore, the AMD simulation can describe the shell effect and the clustering degrees of freedom in the dynamical production of fragments such as a large cross section of the dynamical production of α particles [12,15,16]. Hence, by using the AMD method, we can study the fragmentation mechanism related to nuclear structure [16,17] such as a clustering structure of the ^{19}B nucleus.

In the previous paper [17], we investigated the fragmentation mechanism reflecting the cluster structure of ^{19}B by comparing ^{19}B fragmentation with ^{13}B fragmentation in ^{14}N -target reactions at 35 MeV/nucleon calculated by the AMD method. We have found that there is the abundance of He and Li isotopes in ^{19}B fragmentation compared with those in ^{13}B fragmentation, and that most of the He and Li isotopes are produced simultaneously during dynamical processes in ^{19}B fragmentation. From this result, we have suggested that there is the possibility that the clustering structure of ^{19}B in its ground state can be verified experimentally by conducting a coincident experiment between He and Li isotopes. In this paper, we investigate the incident-energy dependence of ^{19}B and ^{13}B fragmentation in ^{14}N -target reactions using the AMD method combined with a statistical decay calculation, and make clear how the cluster structure of the ^{19}B nucleus is reflected in the final observables, and search for a suitable incident energy to verify the clustering structure of the ^{19}B nucleus experimentally.

This paper is organized as follows. In the next section we describe the AMD formalism briefly. Section III shows the properties of the ground states of B isotopes obtained by the AMD method. In Sec. IV we take a general view of ^{19}B and ^{13}B fragmentation, and show the changing reaction mechanism with incident energy. In Sec. V we focus on the simultaneous production of He and Li isotopes and suggest an experimental way to recognize a clustering structure of the ^{19}B nucleus. Finally, we close this paper by giving a summary and conclusions in Sec. VI.

II. BRIEF EXPLANATION OF AMD FORMALISM

The formalism of AMD is described in detail in Ref. [12], and we give only an outline of the AMD method below. In AMD, the wave function of the A -nucleon system $|\Phi\rangle$ is described by a Slater determinant,

$$|\Phi\rangle = \frac{1}{\sqrt{A!}} \det[\varphi_i(j)], \quad (1)$$

where

$$\varphi_i = \phi_{\mathbf{Z}_i} \chi_{\alpha_i} \quad (\alpha_i = p\uparrow, p\downarrow, n\uparrow, n\downarrow) \quad (2)$$

and

$$\phi_{\mathbf{Z}_i} = \left(\frac{2\nu}{\pi}\right)^{3/4} \exp\left[-\nu\left(\mathbf{r} - \frac{\mathbf{Z}_i}{\sqrt{\nu}}\right)^2 + \frac{1}{2}\mathbf{Z}_i^2\right]. \quad (3)$$

Here, χ_{α_i} and $\phi_{\mathbf{Z}_i}$ are spin-isospin and spatial wave functions of the i th single-particle state, respectively. The complex variables $Z = \{\mathbf{Z}_i\}$ represent the centers of Gaussian wave packets. The width parameter ν is independent of time, and we use $\nu = 0.16 \text{ fm}^{-2}$ in the following calculations.

The time development of the variables Z is determined by the time-dependent variational principle, which leads to the equation of motion for Z :

$$i\hbar \sum_{j\tau} C_{i\sigma,j\tau} \frac{d}{dt} Z_{j\tau} = \frac{\partial \mathcal{H}}{\partial Z_{i\sigma}^*} \quad \text{and} \quad \text{c.c.}, \quad (4)$$

$$C_{i\sigma,j\tau} = \frac{\partial^2}{\partial Z_{i\sigma}^* \partial Z_{j\tau}} \ln \langle \Phi(Z) | \Phi(Z) \rangle, \quad (5)$$

where $\sigma, \tau = x, y, z$. The Hamiltonian of system has the form

$$\mathcal{H}(Z, Z^*) = \frac{\langle \Phi(Z) | H | \Phi(Z) \rangle}{\langle \Phi(Z) | \Phi(Z) \rangle} - \frac{3\hbar^2\nu}{2M} A + T_0[A - N_F(Z)]. \quad (6)$$

In this paper we adopt the Gogny force [18] as the effective central force. The second and the third terms on the right hand side of Eq. (6) have been introduced as the correction for the sake of removing the zero-point energies of the center-of-mass motion of fragments. $N_F(Z)$ represents the number of fragments defined in Refs. [12,17]. The value of T_0 should be equal to $3\hbar^2\nu/2M$ in principle, but a slightly changed value (8.8 MeV) is adopted in order to obtain better binding energies of nuclei.

When we apply the AMD method to heavy-ion reactions, the stochastic collision process should be incorporated as the residual interaction. For this purpose, the physical coordinates $W = \{\mathbf{W}_i\}$ have been introduced [12] because the original coordinates Z have no direct meaning for nucleon positions and momenta due to the antisymmetrization. By using W , the stochastic collision process is incorporated in a similar way into QMD. Pauli blocking is automatically introduced because of the existence of the Pauli forbidden region in the space of W . In this paper we use the in-medium nucleon-nucleon cross section of Ref. [19], but nucleon-alpha collisions are switched off.

The simulations of AMD are truncated at a certain time $t = t_{\text{sw}}$. The dynamical stage of the reactions has finished by this time, and some excited fragments have been formed which will emit lighter particles with a long time scale. Such statistical decays of the equilibrated fragments are calculated with a multistep statistical decay code [20] which is similar to the code of Pühlhofer [21]. In this paper we take $t_{\text{sw}} = 210 \text{ fm}/c$.

The wave function for the ground state of colliding nuclei is constructed by searching the parameters Z which minimize

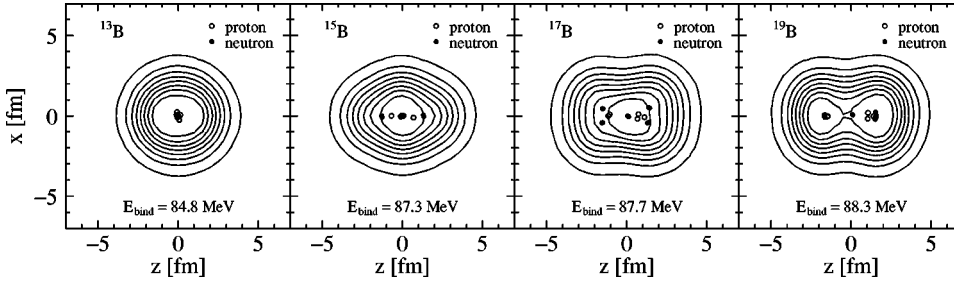


FIG. 1. Density distributions of ground states of B isotopes based on AMD wave functions obtained by the frictional cooling method. Open and solid circles represent the centers of Gaussians of protons and neutrons, respectively.

the expectation value of the Hamiltonian \mathcal{H} . This is done efficiently by using the frictional cooling method [13].

III. GROUND STATES OF B ISOTOPES

Before turning to the main subject, a few remarks should be made concerning the properties of ground states of B isotopes obtained within the AMD framework in the study of Ref. [17]. Density distributions of B isotopes based on the AMD wave functions are displayed in Fig. 1. AMD calculations show the development of cluster structure of B isotopes with an increase of neutron number. The ^{13}B nucleus, which is a neutron closed-shell nucleus, has shell-model-like spherical structure, and cluster structure develops gradually as the neutron number increases, and the ^{19}B nucleus, which is a neutron drip-line nucleus, has a well-developed cluster structure. This development of the clustering structure of B isotopes with an increase of neutron number is considered to be a unique structure in unstable neutron-rich nuclei to bind neutrons as many as possible by a few protons. However, such a clustering structure of neutron-rich nuclei has not been confirmed yet experimentally.

Figure 2 compares AMD calculations with the experimental data about binding energies and root-mean-square radii of ground states of B isotopes, which are shown in the upper and lower panels, respectively. The binding energies of B isotopes are reproduced within the AMD framework quite well, and it should be stressed here that reproduction of the relative binding energies (Q values) is important to describe fragmentation in heavy-ion reactions. The experimental data on the root-mean-square radii of B isotopes are also reproduced quite well by the AMD method. By reflecting the development of the cluster structure in B isotopes, the root-mean-square radii of B isotopes become large with an increase of neutron number.

IV. GENERAL VIEW OF ^{19}B AND ^{13}B FRAGMENTATION

We calculate $^{13}\text{B} + ^{14}\text{N}$ and $^{19}\text{B} + ^{14}\text{N}$ reactions at several incident energies by using the AMD method. Analysis is done for projectilelike fragments, namely, fragments from ^{13}B and ^{19}B nuclei. Projectilelike fragments are recognized based on their velocity component in the beam direction v_z . Figure 3 displays P_z/A distributions of He isotopes produced in $^{13}\text{B} + ^{14}\text{N}$ (left panels) and $^{19}\text{B} + ^{14}\text{N}$ (right panels) reactions at 25, 35, and 55 MeV/nucleon. The fragments with $v_z > v_{NN}$ are regarded as projectilelike fragments, where v_{NN} is the nucleon-nucleon center-of-mass velocity which is indicated in the figure by the arrows inscribed “cut off.”

When the incident energy is beyond 35 MeV/nucleon, the projectilelike and targetlike peaks are clearly seen, and therefore the above procedure for separating projectilelike fragments works well. However, at 25 MeV/nucleon, we cannot separate the projectilelike fragments definitely because of the overlap of the two peaks, so that the above procedure does not work very well at this lowest incident energy.

A. General effects of the projectile property on fragmentation

We show how the difference in character between ^{19}B and ^{13}B nuclei is reflected in their fragmentation.

We have studied in Ref. [17] the case of incident energy 35 MeV/nucleon without taking account of the statistical decay effect. The upper panel of Fig. 4 compares the charge

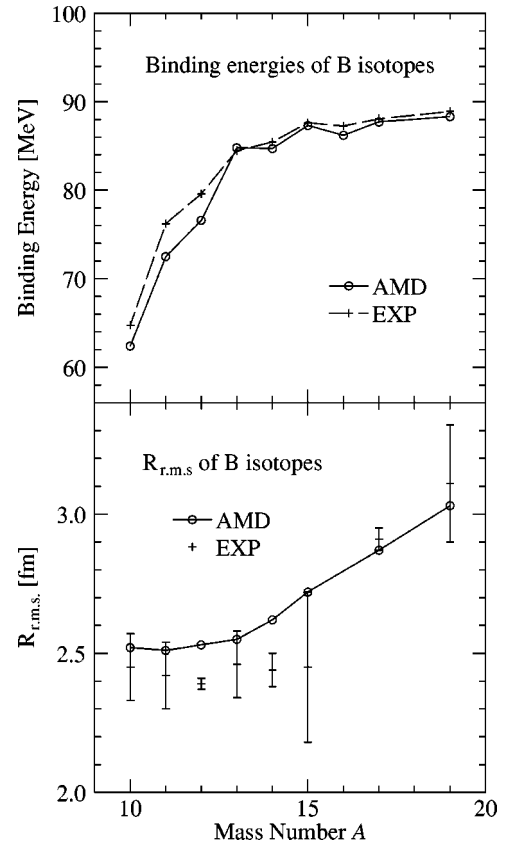


FIG. 2. Comparison of AMD calculations with the experimental data on binding energies and root-mean-square radii of ground states of B isotopes, which are shown in the upper and lower panels, respectively. The solid and dashed lines indicate the AMD calculation and the experimental data, respectively.

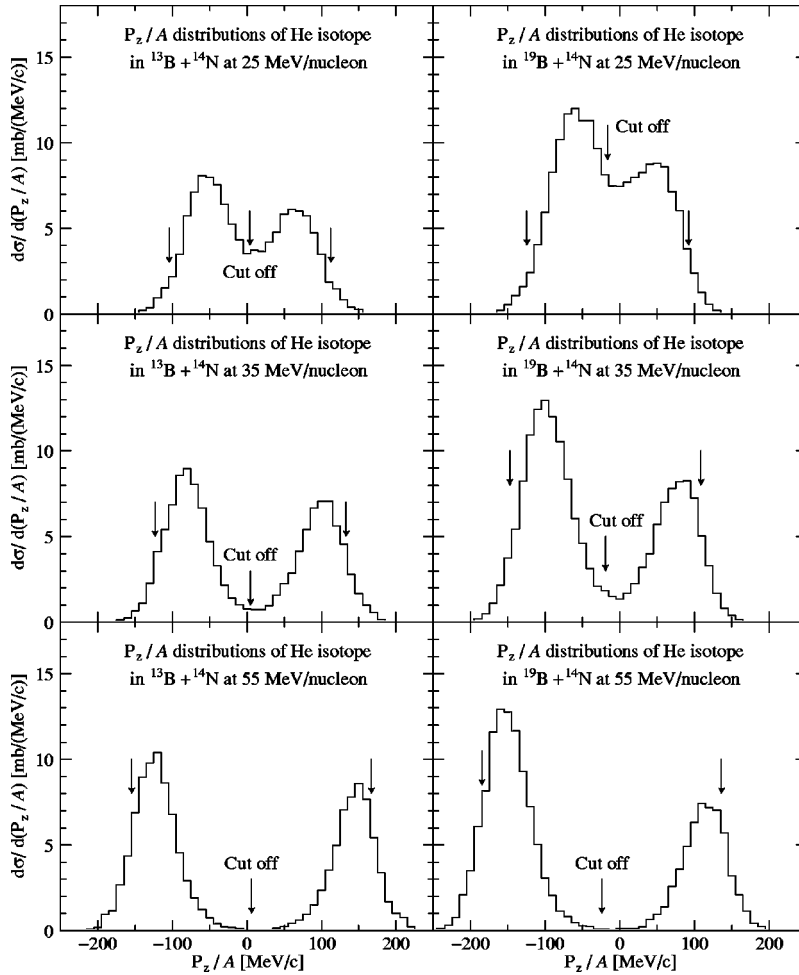


FIG. 3. P_z/A distributions of He isotopes in $^{13}\text{B} + ^{14}\text{N}$ (left panels) and $^{19}\text{B} + ^{14}\text{N}$ (right panels) reactions at 25 (top panels), 35 (middle panels), and 55 (bottom panels) MeV/nucleon. Right and left arrows indicate incident momenta of the projectile, which is ^{13}B or ^{19}B , and the target, which is ^{14}N in these calculations, respectively. Central arrows inscribed “cut off” indicate momenta of nucleon-nucleon center-of-mass systems where AMD simulations are performed in center-of-mass systems.

distribution in ^{19}B fragmentation (solid line) with that in ^{13}B fragmentation (dashed line). We have seen three distinct differences between ^{13}B and ^{19}B fragmentation. The first one is that more He and Li isotopes are produced in ^{19}B fragmentation than in ^{13}B fragmentation, which reflects the cluster structure of ^{19}B . In fact, these He and Li isotopes are produced simultaneously in ^{19}B fragmentation, but not in ^{13}B fragmentation, as shown by the charge distribution in coincidence with the projectilelike Li isotope (lower panel of Fig. 4). The second one is the abundance of fragments with $Z > 5$ in ^{19}B fragmentation compared with those in ^{13}B fragmentation, which reflects the neutron-rich property of ^{19}B . This is because the ^{19}B nucleus approaches the stability line by exchanging neutrons with protons. The third one is related to a loosely bound system of the ^{19}B nucleus with respect to neutron emission. Namely, neutron evaporation from the ^{19}B nucleus should be more preferable than that from the ^{13}B nucleus. Consequently the production cross section of B isotopes in the ^{19}B -induced reaction is larger than that in the ^{13}B -induced reaction. (Note that the contribution of elastic and inelastic scattering is excluded from the production cross section of B isotopes in Fig. 4.)

After statistical decay, as shown in the upper panel of Fig. 5, the characteristic features of the projectile dependence in the charge distribution still remains such as the abundance of He, Li, and C isotopes in ^{19}B fragmentation compared with

^{13}B fragmentation, though the absolute value of the difference is smaller than at the end of dynamical processes (Fig. 4). We can also see from the lower panel of Fig. 5 that a He isotope is often produced in the events with Li production even in ^{13}B fragmentation due to the statistical decay of excited B fragments.

When the incident energy increases up to 100 MeV/nucleon, there is no abundance of He and Li isotopes in ^{19}B fragmentation compared with those in ^{13}B fragmentation even at the end of dynamical processes, as is shown in the upper panel of Fig. 6. Furthermore, as is shown by the coincident charge distributions with the projectilelike Li isotope in the lower panel in Fig. 6, almost all Li isotopes are accompanied by the emission of H isotopes in both ^{13}B and ^{19}B fragmentation. This result indicates that the fragmentation mechanism reflecting the cluster structure of the ^{19}B nucleus depends on the incident energy and information of the cluster structure is lost in the high-incident-energy region.

After statistical decay at 100 MeV/nucleon, we can also see that there is no projectile dependence in both charge and coincident charge distributions (Fig. 7). As a result of the statistical decay of excited B fragments, a He isotope is often produced in events with Li production in both ^{13}B and ^{19}B fragmentation. As for the reflection of the neutron-rich property and the loosely bound system to neutron emission of the

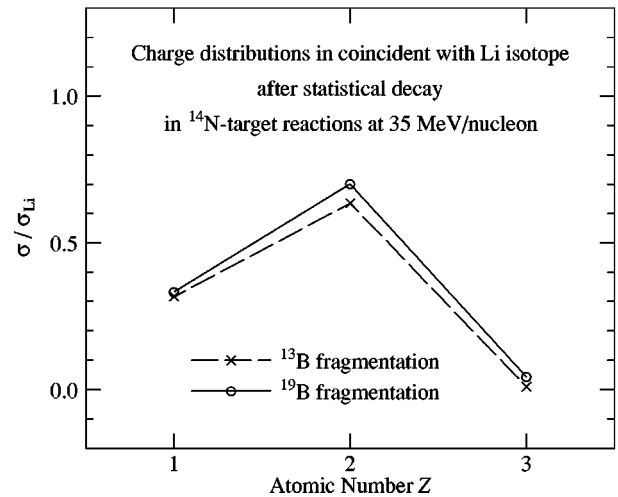
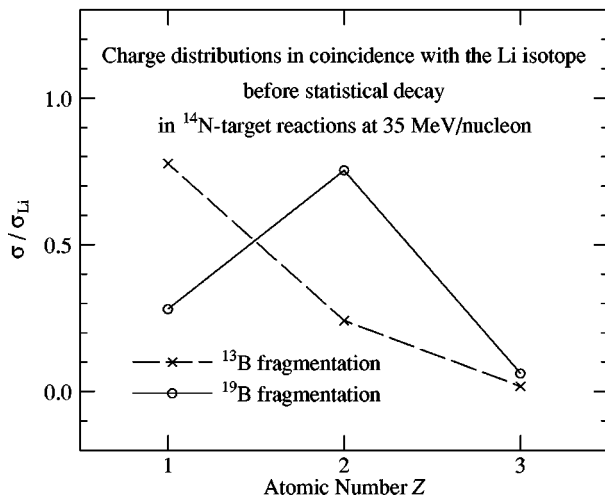
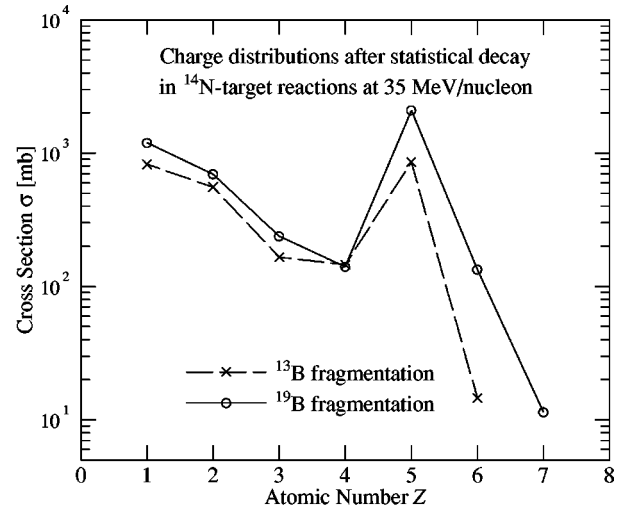
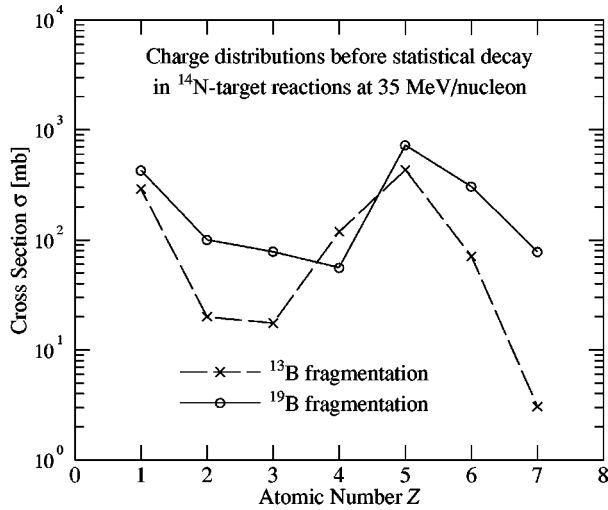


FIG. 4. Charge distributions and coincident charge distributions with the projectilelike Li isotope from ^{13}B and ^{19}B fragmentation at the end of dynamical processes in ^{14}N -target reactions at 35 MeV/nucleon, which are shown in the upper and lower panels, respectively. Solid and dashed lines indicate those from ^{19}B and ^{13}B fragmentation, respectively. The contribution of elastic and inelastic scattering is excluded from the production cross section of B isotopes in charge distributions.

^{19}B nucleus, it remains at 100 MeV/nucleon, which is indicated by an abundance of B and C isotopes in ^{19}B fragmentation compared with those in ^{13}B fragmentation.

B. Changing mechanism of Li production events

In this subsection, we focus only on events in which a projectilelike Li isotope is produced. Figure 8 shows excitation functions of projectilelike Li isotopes in $^{13}\text{B} + ^{14}\text{N}$ and $^{19}\text{B} + ^{14}\text{N}$ reactions, shown by dashed and solid lines, respectively. As we have seen in the previous subsection, at low incident energies around 30 MeV/nucleon, Li isotopes are abundantly produced in ^{19}B fragmentation compared with those in ^{13}B fragmentation. This abundance of Li isotopes in ^{19}B fragmentation becomes small with incident energy increasing, and at 55 MeV/nucleon the difference between ^{19}B

FIG. 5. Charge distributions and coincident charge distributions with the projectilelike Li isotope from ^{13}B and ^{19}B fragmentation after statistical decay in ^{14}N -target reactions at 35 MeV/nucleon, which are shown in the same manner as in Fig. 4.

and ^{13}B fragmentation disappears. This behavior is seen both before and after statistical decay.

In order to see the changing reaction mechanisms producing Li isotopes, we select the events in which a projectilelike Li isotope is produced, and analyze which isotope is produced together with the Li isotope. In Figs. 9 and 10, we plot each fraction of events with H and He or intermediate-mass fragments (IMFs) with $Z \geq 3$ as a function of the incident energy. These figures show the fractions at the end of dynamical processes and after statistical decay, and the upper and lower panels show the cases in ^{13}B and ^{19}B fragmentation, respectively.

As is shown in Fig. 9, the dominant process producing Li isotopes during dynamical processes in ^{13}B fragmentation is the production mechanism accompanied by H isotopes in the whole incident-energy region investigated here. Namely, there is scarcely any correlation among dynamical production of He and Li isotopes in ^{13}B fragmentation at all incident energies, reflecting the fact that the ^{13}B nucleus has no

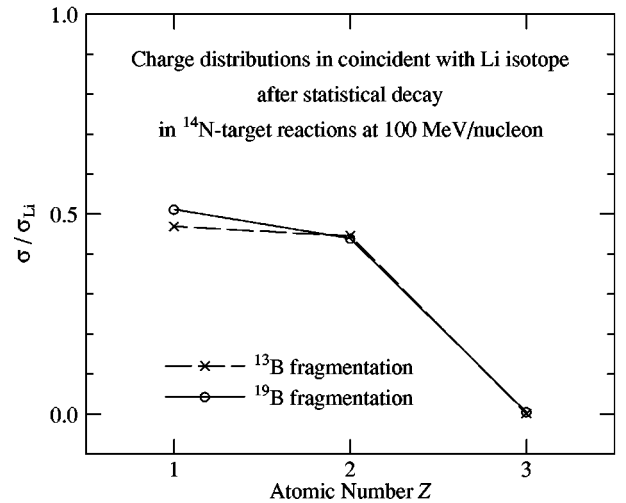
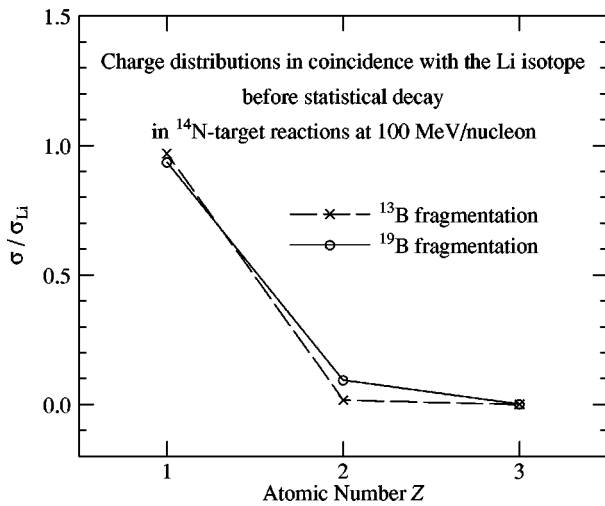
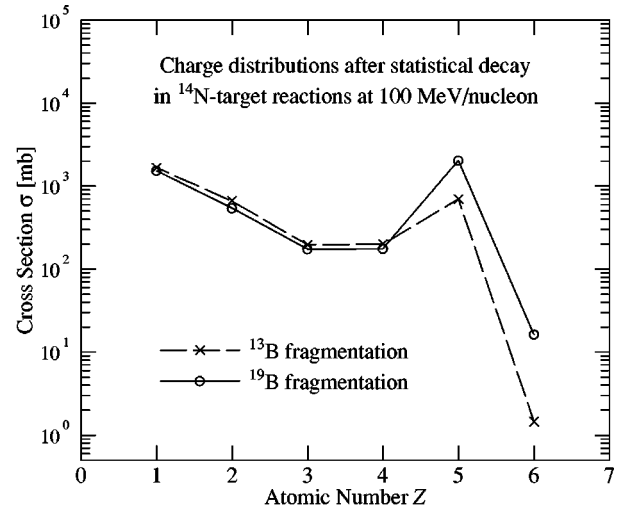
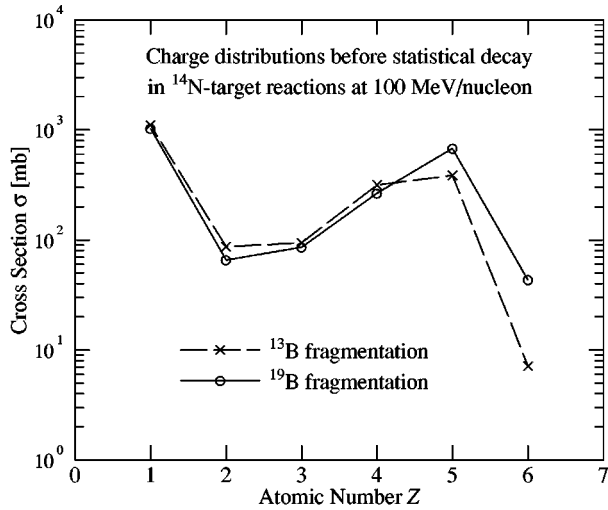


FIG. 6. Charge distributions and coincident charge distributions with the projectilelike Li isotope from ^{13}B and ^{19}B fragmentation at the end of dynamical processes in ^{14}N -target reactions at 100 MeV/nucleon, which are shown in the same manner as in Fig. 4.

seed of clusters in its ground state. On the other hand, in ^{19}B fragmentation, the dominant process producing Li isotopes during dynamical processes is the cluster breakup of ^{19}B into He and Li isotopes in the low-incident-energy region. The fraction of this dynamical cluster breakup reaches up to 80% at 35 MeV/nucleon. This indicates that dynamical cluster breakup of ^{19}B is the origin of the abundance of Li isotopes in ^{19}B fragmentation. The fraction of this dynamical cluster breakup of ^{19}B becomes small with the incident energy increasing, and above ~ 50 MeV/nucleon the dominant process turns to the breakup of ^{19}B into a Li isotopes accompanied with H isotopes as is the same in ^{13}B fragmentation. This means that due to more violent collisions the information of the clustering structure of the ^{19}B nucleus is lost in the higher-incident-energy region.

It should be noticed here that the effect of the neutron-rich property of ^{19}B (namely, the effect of the proton transfer) can be seen also in this analysis. The fraction of the events with an IMF reaches up to 35% at 25 MeV/nucleon in ^{19}B fragmentation, and, on the other hand, this fraction in ^{13}B

FIG. 7. Charge distributions and coincident charge distributions with the projectilelike Li isotope from ^{13}B and ^{19}B fragmentation after statistical decay in ^{14}N -target reactions at 100 MeV/nucleon, which are shown in the same manner as in Fig. 4.

fragmentation reaches up to less than 10% at 25 MeV/nucleon. When the incident energy decreases from 35 MeV/nucleon to 25 MeV/nucleon, the fraction of He events decreases, correlated with the increase of the fraction of IMF events, which indicates that the proton transfer contaminates the dynamical cluster breakup of ^{19}B into He and Li isotopes in the lower-incident-energy region due to the neutron-rich property of the ^{19}B nucleus.

As is shown in Fig. 10, after statistical decay, no difference is found in the classification of events with Li production between ^{13}B and ^{19}B fragmentation. In both cases, the He events have the largest fraction at low incident energies, and this fraction decreases as the incident energy increases. At higher energies, the fraction of He events is similar to that of H events.

V. CLUSTER BREAKUP OF ^{19}B NUCLEUS

Having taken a general view of ^{13}B and ^{19}B fragmentation, we now turn to a detailed investigation of the fragmen-

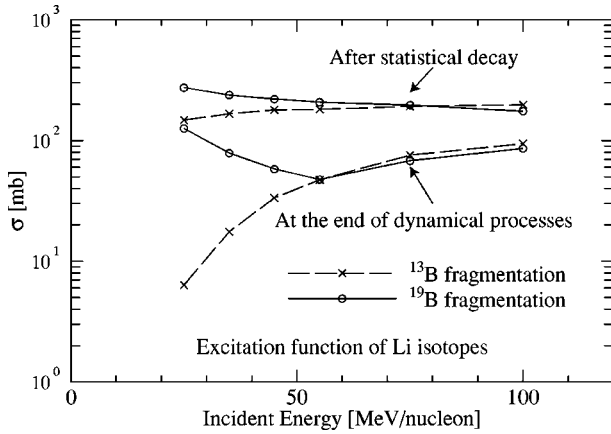


FIG. 8. Excitation functions of the projectilelike Li isotope in $^{19}\text{B} + ^{14}\text{N}$ and $^{13}\text{B} + ^{14}\text{N}$ reactions, which are indicated by solid and dashed lines, respectively. Lower ones indicate those at the end of dynamical processes, and upper ones indicate those after statistical decay.

tation mechanism related to the cluster structure of the ^{19}B nucleus, which is the *dynamical* cluster breakup of ^{19}B into He and Li isotopes. In this section we will study how this dynamical cluster breakup of ^{19}B is reflected in the final

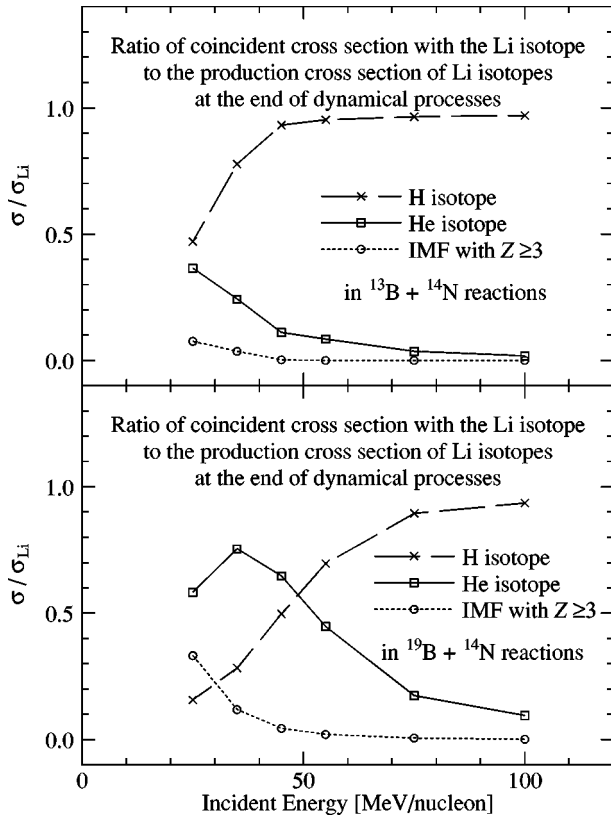


FIG. 9. Ratio of the coincident cross section of the projectilelike Li isotope with H or He isotope or intermediate-mass fragment with $Z \geq 3$ to the production cross section of Li isotopes at the end of dynamical processes, which is indicated by the solid, dashed, or dotted line, respectively. Upper and lower panels show the cases in $^{13}\text{B} + ^{14}\text{N}$ and $^{19}\text{B} + ^{14}\text{N}$ reactions, respectively.

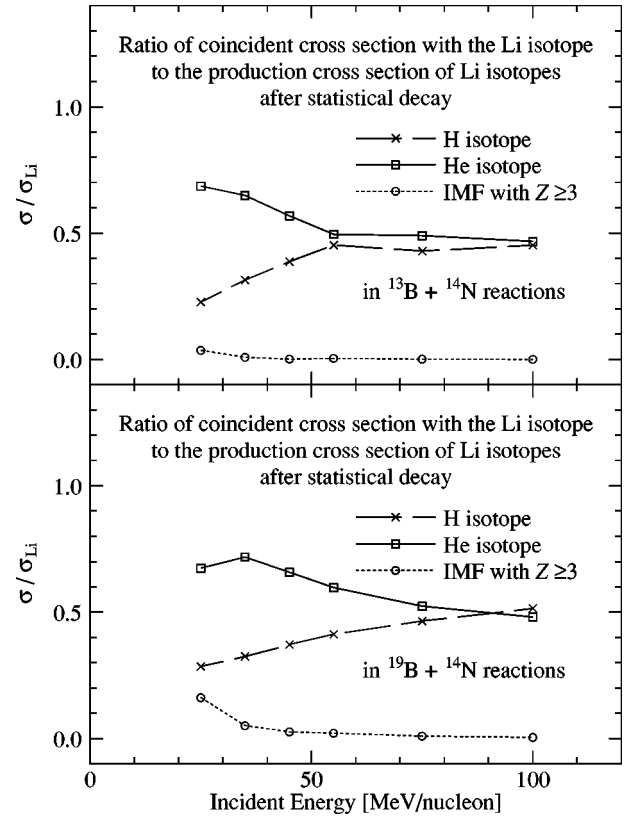


FIG. 10. Ratio of the coincident cross section of the projectilelike Li isotope with H or He isotope or intermediate-mass fragment with $Z \geq 3$ to the production cross section of Li isotopes after statistical decay, which is shown in the same manner as in Fig. 9.

observables in the ^{13}B and ^{19}B fragmentation reactions, and suggest an experimental way to recognize the cluster structure of the ^{19}B nucleus in its ground state by the use of the fragmentation mechanism.

A. Coincident cross section between He and Li isotopes

As a beginning, in Fig. 11, we show the incident-energy dependence of the simultaneous production of projectilelike He and Li isotopes in $^{13}\text{B} + ^{14}\text{N}$ and $^{19}\text{B} + ^{14}\text{N}$ reactions. The upper panel shows the coincident cross section of He and Li isotopes in ^{13}B and ^{19}B fragmentation, which are denoted by dashed and solid lines, respectively. In ^{13}B fragmentation, the coincident cross section hardly depends on the incident energy, while in the case of ^{19}B fragmentation it decreases with an increase of incident energy. At 25 MeV/nucleon the coincident cross section in ^{19}B fragmentation is about twice as large as that in ^{13}B fragmentation, and its difference becomes small as the incident energy increases, and they are almost the same as each other at 100 MeV/nucleon.

The dynamical fraction of the coincident cross sections between He and Li isotopes is shown in the lower panel of Fig. 11. In the case of ^{19}B fragmentation, it can be seen that almost 40% of the coincident pair of He and Li isotopes have already been produced during the dynamical process at $E/A = 25$ MeV/nucleon, and this fraction decreases as the

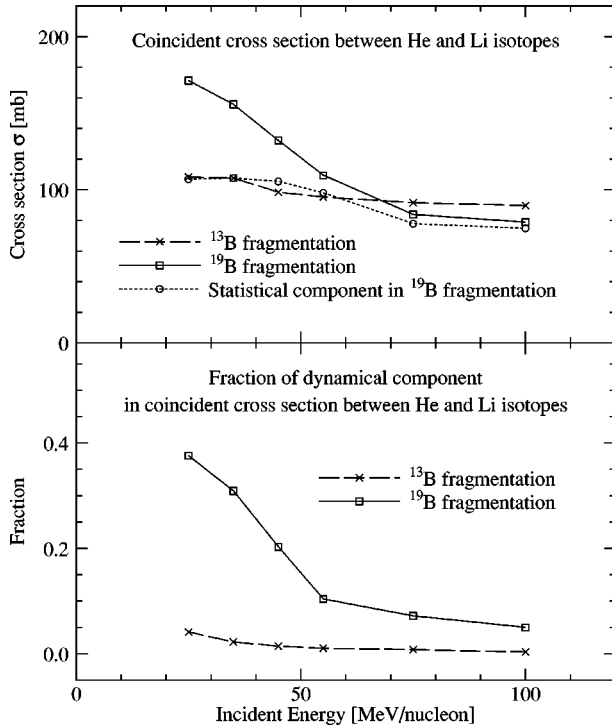


FIG. 11. The upper panel shows the incident-energy dependence of coincident cross sections between He and Li isotopes after statistical decay in $^{13}\text{B} + ^{14}\text{N}$ and $^{19}\text{B} + ^{14}\text{N}$ reactions, which are indicated by dashed and solid lines, respectively. The dotted line indicates the statistical component of the coincident cross section in $^{19}\text{B} + ^{14}\text{N}$ reactions. The lower panel shows the fraction of the dynamical component of the coincident cross sections between He and Li isotopes in $^{13}\text{B} + ^{14}\text{N}$ and $^{19}\text{B} + ^{14}\text{N}$ reactions, which are indicated by dashed and solid lines, respectively.

incident energy increases. On the other hand, in ^{13}B fragmentation, the dynamical fraction is always very small. The dotted line in the upper panel of Fig. 11 indicates the statistical component of the coincident cross section in ^{19}B fragmentation. As is clearly seen, it is as small as the coincident cross section in ^{13}B fragmentation where the statistical component is dominant in the whole incident-energy region. Therefore we can say that because of the *dynamical* cluster breakup of ^{19}B the coincident cross section of He and Li isotopes in ^{19}B fragmentation becomes larger than that in ^{13}B fragmentation at low incident energies, and its difference disappears in the high-incident-energy region since, in both ^{13}B and ^{19}B fragmentation, the simultaneous production of He and Li isotopes is almost due to the statistical decay of excited B isotopes at the end of dynamical processes.

Accordingly we suggest here a coincident experiment between He and Li isotopes as an experimental way to confirm whether the ^{19}B nucleus has cluster structure in its ground state or not. AMD results indicate that, if we observe that the coincident cross section between He and Li isotopes in ^{19}B fragmentation is larger than that in ^{13}B fragmentation at low incident energies around 30 MeV/nucleon, it results from the *dynamical* cluster breakup of ^{19}B by reflecting the cluster structure of the ^{19}B nucleus in its ground state.

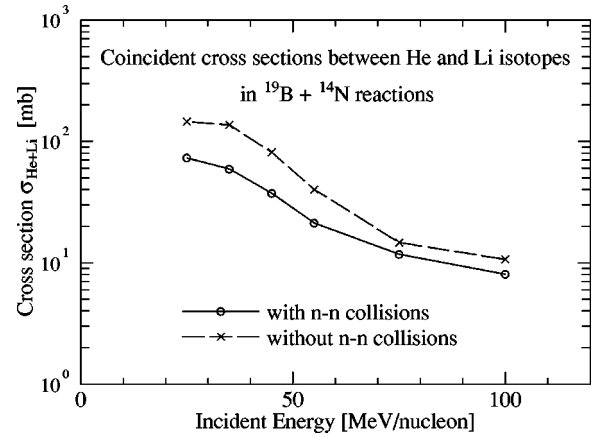


FIG. 12. Incident-energy dependence of coincident cross sections between He and Li isotopes at the end of dynamical processes in $^{19}\text{B} + ^{14}\text{N}$ reactions with and without nucleon-nucleon collision processes, which are indicated by solid and dashed lines, respectively.

B. Effect of the mean field from the target and nucleon-nucleon collision processes

Let us consider here the incident-energy dependence of this dynamical cluster breakup of ^{19}B in terms of the competition between the mean-field effect and nucleon-nucleon collision processes. In order to extract the mean-field effect in the AMD calculation, we perform AMD simulations switching off nucleon-nucleon collision processes. Figure 12 compares coincident cross sections between He and Li isotopes in $^{19}\text{B} + ^{14}\text{N}$ reactions with and without nucleon-nucleon collision processes, which are indicated by solid and dashed lines, respectively. In the low-incident-energy region the coincident cross section without nucleon-nucleon collision processes is much larger than that with nucleon-nucleon collision processes. From this result, we can find that the mean field from the target causes the dynamical cluster breakup of ^{19}B , and, on the other hand, nucleon-nucleon collision processes work to destroy constituent clusters of the ^{19}B nucleus. As the incident energy increases, coincident cross sections between He and Li isotopes decrease monotonously in both cases.

Now we are able to explain such an incident-energy dependence of the coincident cross section in terms of the competition between the mean-field effect and nucleon-nucleon collision processes. In the low-incident-energy region around the Fermi energy, the ^{19}B nucleus can get enough perturbation to break up into He and Li clusters from the mean field of the target and they survive with large probability even if nucleon-nucleon collision processes are included. As the incident energy increases, the ^{19}B nucleus is not disturbed by the mean field from the target enough to break up into He and Li clusters because the interaction time becomes short, and, as a result, the coincident cross section decreases with the incident energy increasing.

C. Impact-parameter dependence of multiplicity of Li isotopes

For the moment let us look closely at the impact-parameter dependence of fragmentation mechanism reflect-

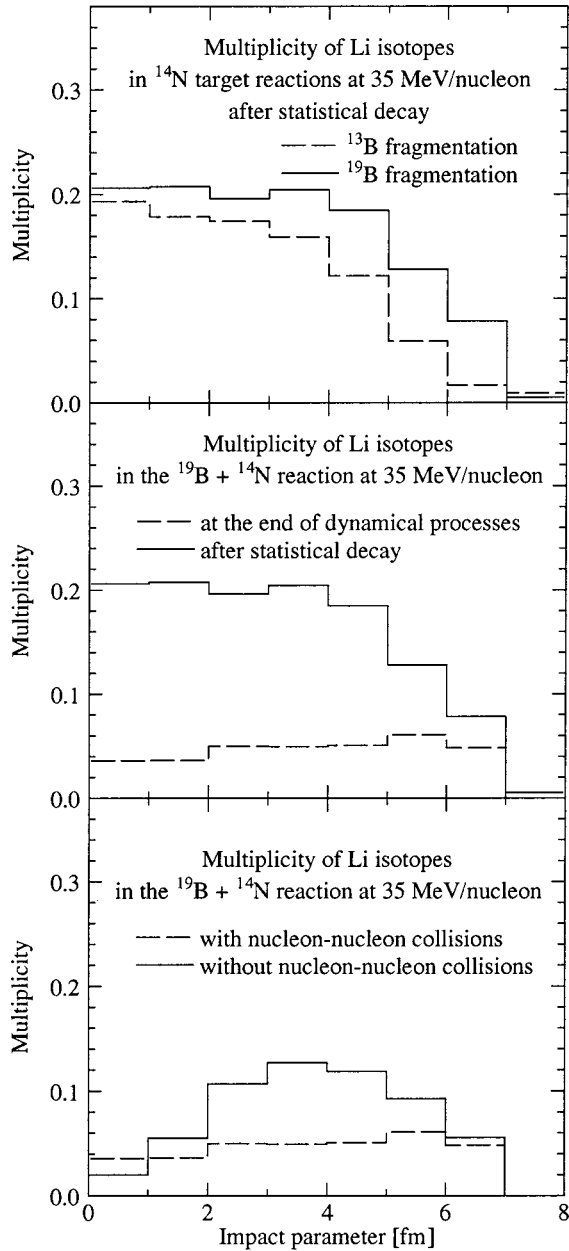


FIG. 13. Top: impact-parameter dependence of the multiplicity of Li isotopes after statistical decay in $^{13}\text{B} + ^{14}\text{N}$ and $^{19}\text{B} + ^{14}\text{N}$ reactions at 35 MeV/nucleon, which are indicated by dashed and solid lines, respectively. Middle: impact-parameter dependence of the multiplicity of Li isotopes at the end of dynamical process and after statistical decay in the $^{19}\text{B} + ^{14}\text{N}$ reaction at 35 MeV/nucleon, which are indicated by dashed and solid lines, respectively. Bottom: impact-parameter dependence of the multiplicity of Li isotopes at the end of dynamical processes in the $^{19}\text{B} + ^{14}\text{N}$ reaction at 35 MeV/nucleon with and without nucleon-nucleon collisions, which are indicated by dashed and solid lines, respectively.

ing the cluster structure of the ^{19}B nucleus. The top panel of Fig. 13 shows the impact-parameter dependence of multiplicity of the projectilelike Li isotope in $^{13}\text{B} + ^{14}\text{N}$ and $^{19}\text{B} + ^{14}\text{N}$ reactions at 35 MeV/nucleon, which are indicated by dashed and solid lines, respectively. At central collisions from 0 to 3 fm, there is only a little difference between ^{13}B

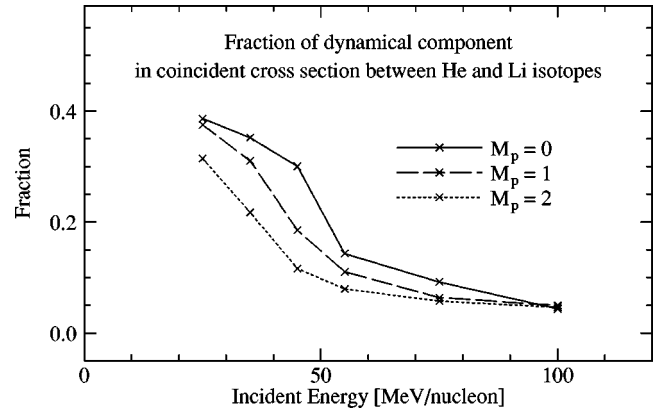


FIG. 14. Fraction of the dynamical component in the coincident cross section between He and Li isotopes in $^{19}\text{B} + ^{14}\text{N}$ reactions. Solid, dashed, and dotted lines denote those selected by the multiplicity of proton from the ^{14}N target, $M_p = 0$, $M_p = 1$, and $M_p = 2$, respectively.

and ^{19}B fragmentation, and its difference becomes large with an increase of the impact parameter. The middle panel compares the projectilelike Li multiplicity at the end of dynamical processes with that after statistical decay in the $^{19}\text{B} + ^{14}\text{N}$ reaction at 35 MeV/nucleon. We can see that peripheral events are preferable in order to extract the dynamical production of Li isotopes, most of which arise from the dynamical cluster breakup reflecting the cluster structure of ^{19}B . It should be recalled here that, as was shown in Fig. 9, 80% of dynamical Li production is due to the dynamical cluster breakup of ^{19}B for the incident energy 35 MeV/nucleon. The bottom panel shows the effects of the mean field and the nucleon-nucleon collisions. Dashed and solid lines indicate cases with and without nucleon-nucleon collision processes for the incident energy 35 MeV/nucleon. It should be noticed that all Li isotopes arise from the dynamical cluster breakup of ^{19}B if nucleon-nucleon collisions are switched off. Without nucleon-nucleon collision processes, the dynamical cluster breakup of ^{19}B occurs at semiperipheral collisions around 3–5 fm most frequently. It is considered that adequate perturbation from the mean field of the ^{14}N target may be necessary for the ^{19}B nucleus to break up into He and Li isotopes during dynamical processes. This peak at semiperipheral collisions disappears with inclusion of nucleon-nucleon collision processes. This is because more nucleon-nucleon collisions occur at more central collisions, and the constituent clusters of the ^{19}B nucleus are destroyed more frequently at more central collisions by nucleon-nucleon collisions.

Accordingly, we expect that the dynamical cluster breakup of ^{19}B can be enhanced further by selecting peripheral events or events with a small number of nucleon-nucleon collisions. For this purpose, we adopt the multiplicity of protons from the ^{14}N target, M_p , for the event sorting. Figure 14 shows dynamical fractions of the coincident cross section between He and Li isotopes filtered by M_p in $^{19}\text{B} + ^{14}\text{N}$ reactions as a function of incident energy. Solid, dashed, and dotted lines denote those selected by $M_p = 0$, $M_p = 1$, and $M_p = 2$, respectively. We can see that the

fraction of the dynamical component becomes large with M_p low. The multiplicity of protons from the target, M_p , is an index of the violence of reactions and low- M_p events correspond to calm reactions. Therefore we find that the ^{19}B nucleus breaks up into He and Li isotopes during dynamical processes in calm reactions, and that low- M_p events are of a somewhat advantage to the dynamical cluster breakup of ^{19}B .

VI. SUMMARY AND CONCLUSION

We investigated the fragmentation mechanism reflecting the cluster structure of the ^{19}B nucleus by calculating $^{19}\text{B} + ^{14}\text{N}$ and $^{13}\text{B} + ^{14}\text{N}$ reactions at several incident energies with the AMD method where the ^{19}B nucleus has a well-developed cluster structure, while the ^{13}B nucleus has no seed of clusters in its ground state. By comparing ^{19}B fragmentation with ^{13}B fragmentation, we found that the cluster structure of ^{19}B is reflected as the dynamical cluster breakup of ^{19}B into He and Li isotopes in its fragmentation. This dynamical cluster breakup of ^{19}B depends on the incident energy. In the low-incident-energy region, the dynamical cluster breakup of ^{19}B occurs and brings about the abundance of He and Li isotopes in ^{19}B fragmentation compared with those in ^{13}B fragmentation. In the high-incident-energy region, the dynamical cluster breakup of ^{19}B hardly occurs, and information of the cluster structure of the ^{19}B nucleus is not included in the final observables due to more violent collisions.

This incident-energy dependence of the dynamical cluster breakup is explained in terms of the competition between the mean-field effect and nucleon-nucleon collision processes. The mean field from the target makes the ^{19}B nucleus break up into He and Li isotopes, while nucleon-nucleon collision processes work to destroy constituent clusters of the ^{19}B nucleus. In the low-incident-energy region, the ^{19}B nucleus can get enough perturbation to break up into constituent clusters from the mean field of the target, and these clusters survive from the destructive effect of nucleon-nucleon collision processes enough to be able to observe the difference in structure between ^{13}B and ^{19}B nuclei.

Furthermore, the dynamical cluster breakup of ^{19}B depends on the impact parameter. Only by the mean field from the target does the ^{19}B nucleus break up into He and Li isotopes at semiperipheral collisions around 3–5 fm most frequently. This indicates that an adequate perturbation from the mean field of the target is necessary for the ^{19}B nucleus

to break up into He and Li isotopes during dynamical processes. With inclusion of nucleon-nucleon collision processes the ^{19}B nucleus breaks up into He and Li isotopes at peripheral collisions most frequently because of the destructive effect of nucleon-nucleon collision processes whose effect is stronger at more central collisions.

From the above results, we suggest that there is the possibility that the clustering structure of the ^{19}B nucleus in its ground state may be verified by the coincident experiment between He and Li isotopes in heavy-ion reactions. AMD results indicate that, if we observe that the coincident cross section in ^{19}B fragmentation is larger than that in ^{13}B fragmentation, it results from the *dynamical* cluster breakup of ^{19}B by reflecting the cluster structure of ^{19}B . By investigating the incident-energy dependence, we found that the difference arising from the difference in structure between ^{13}B and ^{19}B nuclei is seen strikingly when the incident energy is around 30 MeV/nucleon. It is also expected that it may be more advantageous to use a target with large mass because the dynamical cluster breakup of ^{19}B is caused by the mean field from the target whose effect becomes larger with the mass of target larger. Moreover, by observing the multiplicity of protons from the target, low-multiplicity events, which indicate that reactions are calm, are somewhat of an advantage to the dynamical cluster breakup of ^{19}B .

However, the coincident experiment for the verification of the cluster structure of ^{19}B suggested here is hard to realize in the present situation because the ^{19}B nucleus is a neutron drip-line nucleus and the intensity of the secondary beam is too weak to perform this kind of coincident experiments. The clustering structure of B isotopes is expected to develop with the neutron number increasing. Therefore we must investigate how sensitive the dynamical cluster breakup of B isotopes is to the development of cluster structure, and search for the possibility of a coincident experiment to verify the cluster structure of neutron-rich nuclei by the use of the ^{17}B beam. Furthermore, the deformation of B isotopes also becomes large with the neutron number increasing. Therefore we need perform not only a coincident experiment but also a γ spectroscopic experiment in order to verify deformation. These kinds of experiments give us various interesting information for unstable nuclei.

ACKNOWLEDGMENTS

The authors would like to thank H. Sakurai for useful discussions. Most of the computer calculations for this work were performed with the Fujitsu VPP700 at RIKEN, Japan.

-
- [1] *Proceedings of the Fourth International Conference on Radioactive Nuclear Beams*, Omiya, Japan, 1996, edited by S. Kubono, T. Kobayashi, and I. Tanihata [Nucl. Phys. **A616**, 1c (1997)].
- [2] *Proceedings of the First International Conference on Exotic Nuclei and on Atomic Masses*, Arles, France, 1995, edited by M. de Saint Simon and O. Sorlin (Edition Frontières, Gif-sur-Yvette, 1995).

- [3] *Proceedings of the International Symposium on Physics of Unstable Nuclei*, Niigata, 1994, edited by H. Horiuchi, K. Ikeda, K. Sato, Y. Suzuki, and I. Tanihata [Nucl. Phys. **A588**, 1c (1995)].
- [4] H. Okuno, K. Asahi, H. Ueno, H. Sato, M. Adachi, T. Kubo, T. Nakamura, N. Inabe, A. Yoshida, Y. Ohkubo, T. Ichihara, M. Ishihara, T. Shimoda, H. Miyatake, and N. Takahashi, *Hyperfine Interact.* **78**, 97 (1993).

- [5] K. Asahi, H. Ueno, H. Izumi, H. Okuno, K. Nagata, H. Ogawa, Y. Hori, H. Sato, K. Mochinaga, M. Adachi, A. Yoshida, G. Liu, N. Aoi, T. Kubo, M. Ishihara, W. D. Schmidt-Ott, T. Shimoda, H. Miyatake, S. Mituoka, and N. Takahashi, in *Proceedings of the International Symposium on Physics of Unstable Nuclei* [3], p. 135c
- [6] M. Seya, M. Kohno, and S. Nagata, *Prog. Theor. Phys.* **65**, 204 (1981).
- [7] H. Furutani, H. Kanada, T. Kaneko, S. Nagata, H. Nishioka, S. Okabe, S. Saito, T. Sakuda, and M. Seya, *Suppl. Prog. Theor. Phys.* **68**, 193 (1980).
- [8] Y. Kanada-En'yo and H. Horiuchi, *Phys. Rev. C* **52**, 647 (1995).
- [9] M. Freer, J. C. Angélique, L. Axelsson, B. Benoit, U. Bergmann, W. N. Carford, S. P. G. Chappell, N. M. Clarke, N. Curtis, A. D'Arrigo, E. de Goes Brennard, O. Dorvaux, B. R. Fulton, G. Giardina, C. Gregori, S. Grévy, F. Hanappe, G. Kelly, M. Labiche, C. Le Brun, S. Leenhardt, M. Lewitowicz, K. Markenroth, F. M. Marqués, M. Motta, J. T. Murgatroyd, T. Nilsson, A. Ninane, N. A. Orr, I. Piqueras, M. G. Saint Laurent, S. M. Singer, O. Sorlin, L. Stuttgé, and D. L. Watson, *Phys. Rev. Lett.* **82**, 1383 (1999).
- [10] G. F. Bertsch and S. Das Gupta, *Phys. Rep.* **160**, 189 (1988).
- [11] J. Aichelin and H. Stöcker, *Phys. Lett. B* **176**, 14 (1986); J. Aichelin, *Phys. Rep.* **202**, 283 (1991).
- [12] A. Ono, H. Horiuchi, T. Maruyama, and A. Ohnishi, *Prog. Theor. Phys.* **87**, 1185 (1992).
- [13] Y. Kanada-En'yo and H. Horiuchi, *Prog. Theor. Phys.* **93**, 115 (1995).
- [14] A. Doté, H. Horiuchi, and Y. Kanada-En'yo, *Phys. Rev. C* **56**, 1844 (1997).
- [15] A. Ono and H. Horiuchi, *Phys. Rev. C* **51**, 299 (1995).
- [16] H. Takemoto, H. Horiuchi, A. Engel, and A. Ono, *Phys. Rev. C* **54**, 266 (1996); H. Takemoto, H. Horiuchi, and A. Ono, *ibid.* **57**, 811 (1998).
- [17] H. Takemoto, H. Horiuchi, and A. Ono, *Prog. Theor. Phys.* **101**, 101 (1999).
- [18] J. Dechargé and D. Gogny, *Phys. Rev. C* **21**, 1568 (1980).
- [19] A. Ono, H. Horiuchi, and T. Maruyama, *Phys. Rev. C* **48**, 2946 (1993).
- [20] Toshiaki Maruyama, A. Ono, A. Ohnishi, and H. Horiuchi, *Prog. Theor. Phys.* **87**, 1367 (1992).
- [21] F. Pühlhofer, *Nucl. Phys.* **A280**, 267 (1977).